ADVANCED FUNCTIONAL MATERIALS
www.afm-journal.de

Vitamins as Active Agents for Highly Emissive and Stable Nanostructured Halide Perovskite Inks and 3D Composites Fabricated by Additive Manufacturing

Ileana Recalde, Andrés. F. Gualdrón-Reyes, Carlos Echeverría-Arrondo, Alexis Villanueva-Antolí, Jorge Simancas, Jhonatan Rodriguez-Pereira, Marcileia Zanatta, Iván Mora-Seró,* and Victor Sans**

The use of non-toxic and low-cost vitamins like α-tocopherol (α-TCP, vitamin E) to improve the photophysical properties and stability of perovskite nanocrystals (PNCs), through post-synthetic ligand surface passivation, is demonstrated for the first time. Especially interesting is its effect on $CsPbI_3$ the most unstable inorganic PNC. Adding α-TCP produces that the photoluminescence quantum yield (PLQY) of freshly prepared and aged PNCs achieves values of ≈98% and 100%, respectively. After storing 2 months under ambient air and 60% relative humidity, PLQY is maintained at 85% and 67%, respectively. α-TCP restores the PL features of aged $CsPbI_3$ PNCs, and mediates the radiative recombination channels by reducing surface defects. In addition, the combination of α-TCP and PNCs facilitates the chemical formulation to prepare PNCs-acrylic polymer composites processable by additive manufacturing. This enables the development of complex shaped parts with improved luminescent features and long-term stability for 4 months, which is not possible for non-modified PNCs. A PLQY ≈92% is reached in the 3D printed polymer/PNC composite, the highest value obtained for a red-emitting composite solid until now as far as it is known. The passivation shell provided by α-TCP makes that PNCs inks do not suffer any degradation process avoiding the contact with the environment and preserve their properties after reacting with polar monomers during composite polymerization.

1. Introduction

After less than one decade of the first synthesis reports,[1,2] perovskite nanocrystals (PNCs) continue being the most attractive luminescent materials, due to their intrinsic properties.[3] A photoluminescence quantum yield (PLQY) up to 100%,[4–6] narrow full width and half maximum photoluminescence (PL),[7] high tolerance-to-defect structure,[8] dynamic surface chemistry,[9] facile preparation by diverse synthetic protocols and composition/size engineering to modulate the bandgap,[6,10,11] are the most outstanding characteristics that have been studied in optoelectronics and photovoltaics. More interestingly, the nanoconfinement regime that PNCs present enables the stabilization of photoactive crystalline phases under ambient air.[12,13] Thus, PNCs have gained preference over the bulk perovskites, where non-photoactive crystalline δ-phase is more prone to be formed.[12,14] This is the case of iodide-based PNCs

I. Recalde, A. F. Gualdrón-Reyes, C. Echeverría-Arrondo, A. Villanueva-Antolí, J. Simancas, M. Zanatta, I. Mora-Seró, V. Sans
Institute of Advanced Materials (INAM)
Universitat Jaume I (UJI)
Avenida de Vicent Sos Baynat, s/n
Castelló de la Plana, Castellón 12071, Spain
E-mail: andres.gualdron@uach.cl; sero@uji.es; sans@uji.es

The ORCID identification number(s) for the author(s) of this article can be found under https://doi.org/10.1002/adfm.202210802.

DOI: 10.1002/adfm.202210802

A. F. Gualdrón-Reyes
Facultad de Ciencias
Instituto de Ciencias Químicas
Isla Teja
Universidad Austral de Chile
Valdivia 5090000, Chile

J. Rodriguez-Pereira
Center of Materials and Nanotechnologies
Faculty of Chemical Technology
University of Pardubice
Nam. Cs. Legii 565, Pardubice 53002, Czech Republic

J. Rodriguez-Pereira
Central European Institute of Technology
Brno University of Technology
Purkyňova 123, Brno 612 00, Czech Republic

(I-PNCs) such as $CsPbI_3$ and $FAPbI_3$ (FA; formamidinium), which depict an optical bandgap ≈1.7 and 1.4 eV, respectively, when the black α-phase is obtained,[15] but beyond 2.3 eV for δ-phase.

I-PNCs allow on one hand the emission of pure red and NIR light, and on the other hand the development of light absorbers with the optimum band gap for photovoltaic applications.[16] The maximum theoretical photoconversion efficiency (PCE) has been calculated to be 32.3%, for the case of bulk $FAPbI_3$,[12] close to the theoretical Shockley–Queisser limit. Even though the PCE of I-PNCs is still far from this value, a fast increment up to 18.1% with a long-term stability[17] has been reached in a couple of years. Strategies such as the washing of PNCs with low-polarity antisolvents and the fabrication of PNCs films by layer-by-layer deposition have been suitable strategies to remove some fraction of long-chain capping ligands acting as isolators and to decrease the density of structural defects, thus improving the performance of devices.[18,19]

The nanoconfinement regime can extend the black phase stability of iodide-perovskites. However, aged samples exhibit a decrease in PLQY. The aging process gives time to some capping ligands such as oleic acid (OA) and oleylamine (OLA) to detach from the PNCs surface.[20] This results in the formation of surface defects, mainly halide deficiencies, which deteriorates the PLQY.[4,21] Mostly, the loss of ammonium species such as oleylammonium iodide (OLAm-I) is the main reason to generate halide vacancies (undercoordinated Pb atoms), which causes the tilting of the octahedra in the PNCs lattice, favoring a fast α-to-δ phase transformation, and the emergence of a high density of non-radiative carrier traps.[4,21,22] At this point, the modification of synthetic procedures, ligand engineering, metal-doping, and matrix-encapsulation have been studied as potential alternatives to prepare high-quality I-PNCs with extended stability.[3,6,21] Mainly, the addition of a high content of OA/OLA from the conventional protocol mediates the formation of enough OLAm-I species, dissolve the halide precursor and support the PNCs stabilization.[10]

On the other hand, the partial replacement of Pb^{2+} by a small fraction of Bi^{3+} or Sr^{2+} cations,[4,23] or the use of capping ligands with stronger binding ability, such as trioctylphosphine (TOP) or sulfur-oleylamine, can reduce the density of halide defects in the as-prepared material.[5,24] In the case of TOP, a 100% PLQY can be achieved, with a stability ≈1 month. Interestingly, this ligand has also added to aged $CsPbBr_{3-x}I_x$ PNCs colloidal solutions to recover their PL properties.[25] Nevertheless, phosphines and most of the recent capping ligands used for PNCs stabilization have inherent toxicity, hindering their potential industrial applications.

Even if the structural integrity of PNCs is favored by ligand engineering, their combination with certain solvents to prepare formulations suitable to create complex structures is very challenging. This is the goal of the additive manufacturing, commonly known as 3D printing, which makes use of tailored inks for the generation of macroscopic complex devices typically in a layer-by-layer fashion.[26] In particular, the use of monomeric based formulations, typically acrylate based, is used in stereolithography and digital light processing, to generate highly detailed designs by controlled photopolymerization within a polymerization bath, known as vat. The development of advanced formulations able to stabilize active molecular and nanostructured materials, enables the transfer of their properties, including tailored electrochemical properties,[27] photo-[28] and thermochromism[29] into solid materials and thin layers.[30] This feature is well employed in attractive applications such as quantum dot organic light-emitting diode displays,[31] for the patterning of micro/macro structures and ink-lithography,[32] where the ink is deposited on both rigid and flexible substrates to fabricate a new generation of thin-film transistors, circuits, opening the door to 3D optoelectronics. Nevertheless, the use of polar solvents for ink preparation such as dimethyl sulfoxide, γ-butyrolactone, N-methyl-2-pyrrolidone among others that typically dissolve lead halide precursors,[33,34] can lead to the deterioration of the PLQY of PNCs, especially in the case of I-PNCs that are more prone to α-to-δ phase transformation. Thus, a versatile methodology to stabilize red-emitting PNCs free from etching solvents for the ink's formulation and keep their PL properties after printing process has not been widely exploited.

In this work, we demonstrate for the first time, as far as we know, the use of non-toxic and low-cost vitamins as a very effective strategy to improve the intrinsic features of as-synthesized PNCs in general and in particular of the most demanding I-PNCs and also able to recover the lost properties of aged PNCs. To this end we employed α-tocopherol (α-TCP), the most biologically active form of the vitamin E, which is commonly used as an antioxidant.[35] Ligand passivation of the $CsPbI_3$ PNCs with α-TCP enabled to: 1) provide an efficient passivation to reach a PLQY close to 100%; 2) rmaintain a high PLQY for several at least months under ambient air conditions; 3) recover the PLQY from an aged I-PNCs in a 28%; 4) stabilize I-PNC in polymeric films especially formulated for 3D printing and 5) develop highly emissive inks for 3D printing. We were able to reach a PLQY ≈92% in the 3D printed composite polymer/PNC, which was maintained for 4 months, being this value the highest one obtained for a red-emitting composite polymer/PNCs solid as far as we know.

2. Results and Discussion

Initially, to establish how α-TCP impacts on the intrinsic properties and stability of PNCs, different molar concentrations of this vitamin were added to two different kind of $CsPbI_3$ PNCs samples: i) as-prepared PNCs (P1) and ii) the same material aged for 1 month (P2), hereafter named *X*-T@P1 and *X*-T@P2, respectively, where *X* is the molar concentration of α-TCP. **Figure 1**a,a',b,b' shows the representative transmission electron microscopy (TEM) images of P1 in absence of α-TCP (0-T@P1) and 0.15-T@P1 sample at 0 day and after 60 days aging, respectively. Both as-prepared materials exhibit a nanocube morphology, with an average particle size ≈11.7 and 10.1 nm, respectively, see Figure S1 (Supporting Information). Through Selected area diffraction (SAED) patterns, we show that the presence of α-TCP does not promote any phase transformation, observing the characteristic interplanar spacings of the $CsPbI_3$ cubic phase (ICSD 161 481),[36] see Figure S2 (Supporting Information). Nevertheless, for the 0-T@P1 sample after 60 days aging, a nanowire type morphology is observed, showing characteristic interplanar spacings of the orthorhombic phase

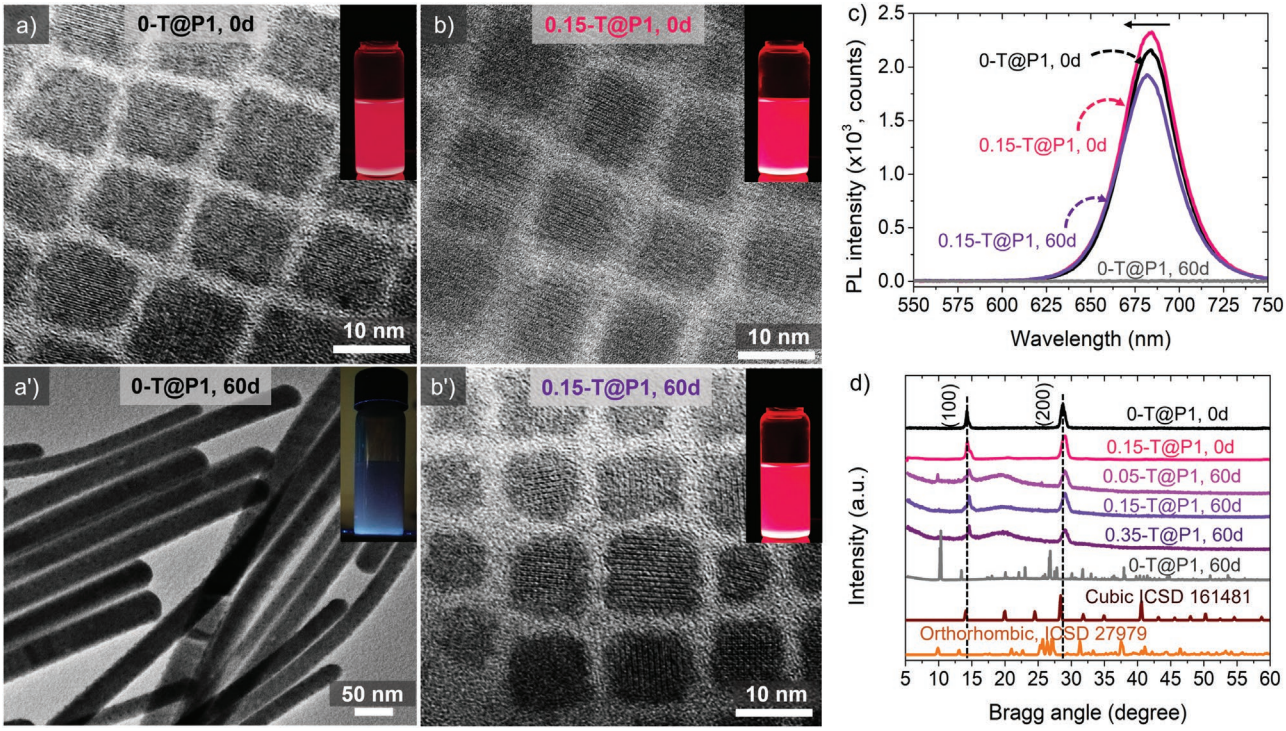

Figure 1. Typical TEM images of a,a') 0-T@P1 and b,b') 0.15-T@P1 at a,b) day 0 and a'b') after 60 d. c) PL spectra of the PNCs samples at different time of aging at ambient conditions, with and without α-TCP. d) XRD patterns of 0-T@P1 and *X*-T@P1 at day 0 and after 60 d by adding different concentrations of α-TCP.

(ICSD 27 979),[37] different from the cubic phase of 0.15-T@P1 under the same aging time. The presence of $CsPbI_3$ nanowires in the absence of α-TCP is typical from the α-to-δ phase transformation induced by lattice distortion, deteriorating the photoactive crystalline of the perovskite.[38] Through the morphological and optical characterization seen in Figure S3 (Supporting Information), it is observed that the partial α-to-δ phase transition starts to occur after 20 days under ambient conditions, inducing the progressive quenching of the optical properties in pristine PNCs. Hence, the inclusion of α-TCP efficiently stabilizes the photoactive cubic phase of PNCs over the time. Figure 1c exhibits the PL spectra of 0-T@P1 and 0.15-T@P1 exposed to the ambient air up to 60 days. Here, the PL intensity of 0.15-T@P1 is higher than that of PNCs in absence of the vitamin and this signal is kept after long time. Meanwhile, the PL feature of 0-T@P1 is totally quenched. This feature indicates that radiative carrier recombination is favored, suggesting that some surface defects produced by the removal of the above-mentioned ligands can interact with α-TCP, thus enhancing the photophysical features and stability of the PNCs.[21,39,40]

Figure 1d shows the typical XRD patterns of *X*-T@P1 at 0 day and 60 days of exposure to the ambient air. After 60 days all the materials with α-TCP, regardless of the concentration, show two main peaks associated to the (100) and (200) planes of cubic phase,[10] similar to the as-prepared 0-T@P1 and 0.15-T@P1 samples. Meanwhile, the PNCs sample without α-TCP has transformed into the orthorhombic phase, indicating that α-TCP inhibits the fast α-to-δ phase transformation. Furthermore, the XRD peaks are displaced to higher Bragg angles in the presence of α-TCP, ascribed to a lattice contraction.[41] At this stage, we can conclude that the delay of the crystalline phase transition is caused by the hindering of the octahedra tilting from the perovskite structure mediated by the α-TCP coverage.

The influence of α-TCP on the surface properties, chemical environment and composition of $CsPbI_3$ PNCs was investigated with X-ray photoelectron spectroscopy (XPS). For this purpose, XPS measurements were conducted to 0-T@P1 and 0.15-T@P1 samples under different aging times (at 0 and 60 days). By obtaining the survey spectra of the materials, we identified the presence of C, N, O, Cs, Pb, and I, see Figure S4 (Supporting Information). The corresponding chemical composition is shown in Table S1 (Supporting Information). **Figure 2**a exhibits the typical high-resolution (HR) XPS Cs 3d spectra of 0-T@P1 and 0.15-T@P1 samples, where a doublet ≈724/738 eV is depicted. These signals are representative of the Cs $3d_{5/2}$ and Cs $3d_{3/2}$ core levels from Cs^+ species contained into the $CsPbI_3$ structure.[42] Additionally, Cs 3d doublets were displaced to higher binding energies (BEs) after α-TCP addition. This fact suggests a compensation of halide deficiency by oxygen coming from α-TCP. Then, 0-T@P1 and 0.15-T@P1 samples with different aging time show Cs^+ deficiency, leading to an alteration of PNCs surface stoichiometry.[20,43] The generation of this kind of defects could explain why 0-T@P1 is prone to suffer the α-to-δ phase transformation in a couple of days, losing their optical properties. Interestingly, the fact that 0.15-T@P1 still presents the characteristic red emission after 2 months indicates that α-TCP improves the stability to the environment after ligand passivation process.

Figure 2b shows the HR-XPS I 3d spectra of 0-T@P1 and 0.15-T@P1 materials. It is observed the presence of the typical

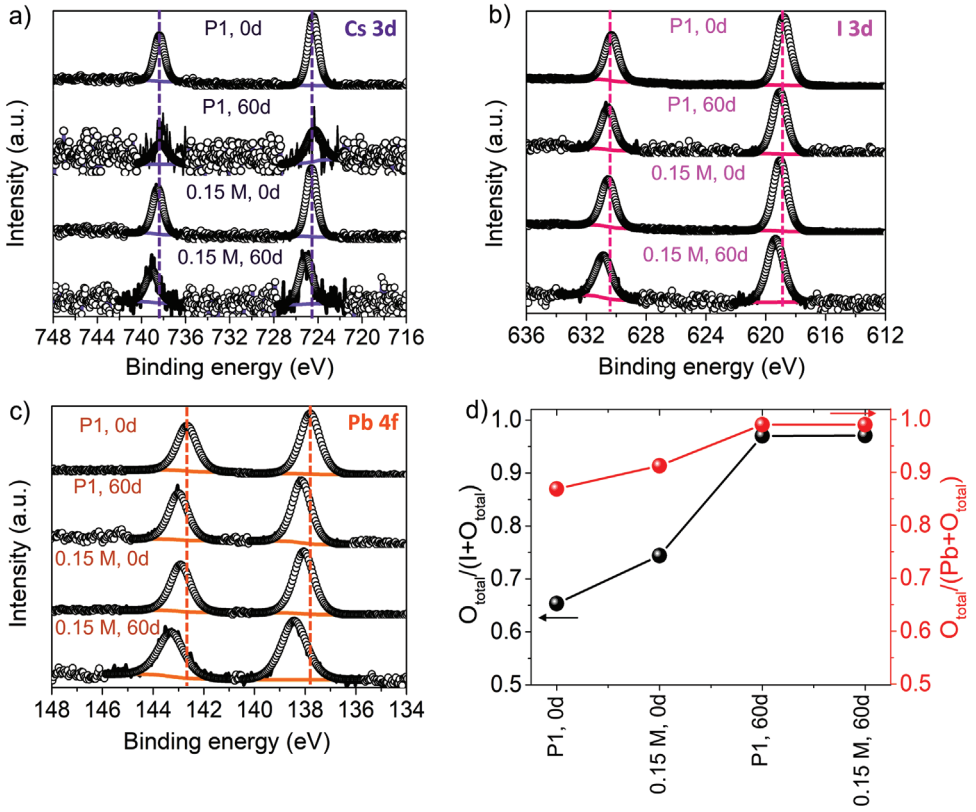

Figure 2. HR-XPS a) Cs 3d, b) I 3d, c) Pb 4f spectra, and d) calculated total oxygen-to-halide and total oxygen-to-lead ratios for 0-T@P1 (P1) and X-T@P1 (X = 0.15 M) samples under different aging time (0 and 60 d).

spin-orbit splitting I $3d_{5/2}$ and I $3d_{3/2}$ peaks at ≈618.3/630 eV, corresponding to the iodide species into $[PbI_6]$ octahedra composing the PNCs.[4,43] Similar to Cs 3d doublet, a displacement to higher BEs was also observed for I 3d peaks in presence of α-TCP. Since oxygen exhibits a higher electronegativity than iodine, oxygen from α-TCP can fill halide vacancies in PNCs, forming new O—Pb—I bonds. Then, iodide content of 0.15-T@P1 after 2 months of aging is slowly decreased than that of 0-T@P1 under the same time. This fact allows to deduce that α-TCP hinders the detachment of iodide species from the PNCs, which is pivotal to enhance their stability.

Figure 2c depicts the HR-XPS Pb 4f spectra of 0-T@P1 and 0.15-T@P1 samples. It is evidenced the characteristic Pb $4f_{7/2}$ and Pb $4f_{5/2}$ core levels attained ≈138/143 eV,[4,43] respectively, showing a shift toward higher BEs, consequence of the incorporation of a more electronegative species into the PNCs. Attending to the chemical composition summarized at Table S1 (Supporting Information), 0-T@P1 at 0 day shows an initial oxygen content accompanied with the absence of undercoordinated Pb. This is associated to the use of methyl acetate as antisolvent during the washing process of the PNCs, which passivates halide defects through COO^- anions.[18] Accordingly, all the PNCs samples should present the same initial oxygen density, referred as oxygen-to-total iodine and oxygen-to-total lead ratios ($O_{total}/I+O_{total}$) and ($O_{total}/Pb+O_{total}$), respectively, see Figure 2d. However, the addition of α-TCP makes that this initial point increase, being higher for 0.15-T@P1 at 0 day. Then, even both the ($O_{total}/I+O_{total}$) and $O_{total}/Pb+O_{total}$) ratios of 0.15-T@P1 presents a variation after 60 days of aging, reaching similar values to a degraded 0-T@P1 under the same aging time, the change of both ratios before and after 60 days (described as $\Delta(O_{total}/I+O_{total})$ and $\Delta(O_{total}/Pb+O_{total})$), Table S1, Supporting Information) for 0.15-T@P1 are lower than for 0-T@P1. This trend allows to confirm that all the chemical environment of the PNCs is modified by oxygen incorporation from α-TCP, concluding that this ligand is linked to the PNCs surface during post-synthetic treatment. As it will be shown below, phenolate anion from α-TCP is the component where this vitamin is linked to the perovskite surface.

Considering that the long-chain capping ligands are detached from the PNCs during the aging process,[11,12,44] the addition of a potential ligand to provide a suitable ligand passivation to as-prepared PNCs and restore the intrinsic properties of aged ones, is pivotal to generate samples with higher quality and prolonged stability. With this hypothesis, the influence of α-TCP on the photophysical properties of $CsPbI_3$ PNCs was studied by adding different content of this vitamin to as-prepared and aged samples. Then, we measured their corresponding PLQY at room temperature under aerobic conditions and relative humidity ≈60%. As seen in **Figure 3**a,b, the PLQY of *X*-T@P1 and *X*-T@P2 samples reach the highest value ≈98 and 100%, respectively, after 6 d in presence of α-TCP. These values were obtained by increasing this vitamin content up to 0.15 M in both cases. Then, the PLQY decreased after adding an excess of this organic. Considering that 0-T@P1 sample show an initial PLQY of ca. 91%, it can be deduced that the presence of α-TCP

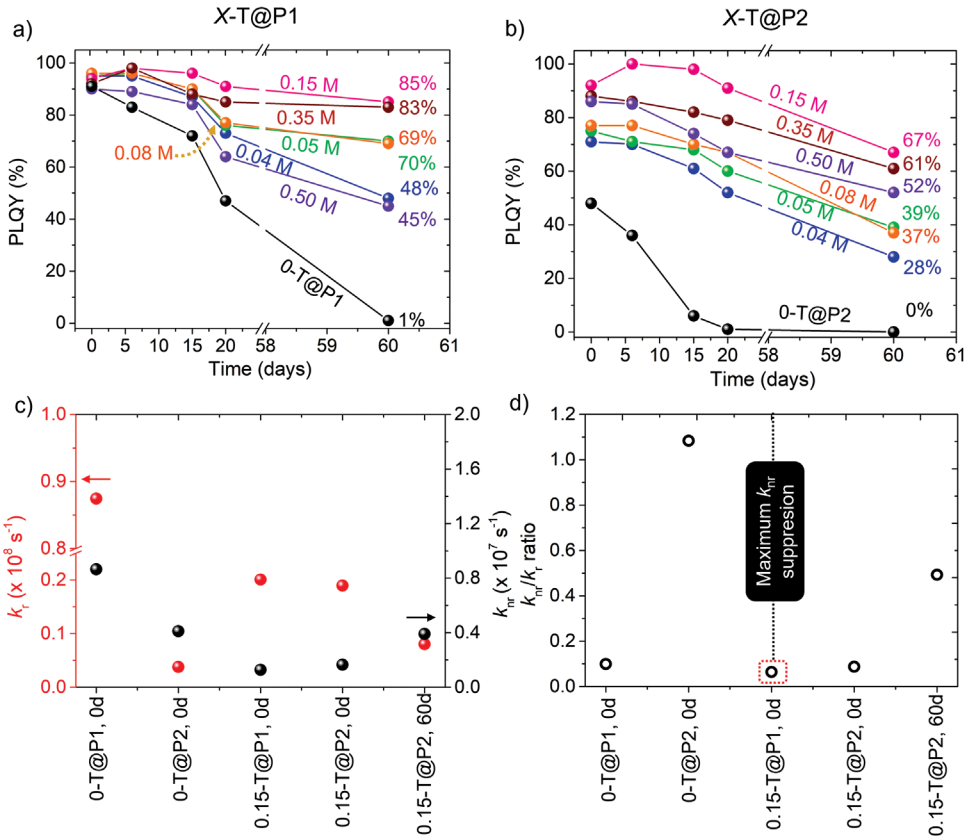

Figure 3. PLQY values as a function of aged days for a) *X*-T@P1 and b) *X*-T@P2 colloidal solutions in absence and presence of different concentration of α-TCP. c) Behavior of radiative (k_r) (red dots), non-radiative recombination (k_{nr}) (black dots) decay constants, and their corresponding d) k_{nr}/k_r ratio.

does not only restrain the α-to-δ phase transformation in the material, but also maximizes the radiative recombination as the main pathway governing the carrier relaxation. This effect has been previously observed by using alternative organic ligands such as didodecyldimethylammonium bromide (DDAB),[45] bidentate,[46] zwitterionic ligands,[47] which are filling or suppressing defects from the PNCs surface. Nevertheless, no previous have been reported the use of these molecules to restore the intrinsic properties of aged $CsPbI_3$ PNCs in a post-synthetic treatment.

Accordingly, this fact suggests that α-TCP, a vitamin that can be isolated from natural sources such as fruits, vegetables, seeds, etc., is not only able to promote the passivation of surface defects in as-prepared PNCs by creating a coverage on the material surface, but also to restore the PLQY of aged samples, compensating structural defects and reducing the non-radiative recombination. The ligand passivation effect of α-TCP is more evident by detailing the PLQY of the *X*-T@P2 samples, which was enhanced with respect to 0-T@P2 material, with an initial low value ≈48%. This fact allows us to infer once more that α-TCP mediates the restoration of PNCs surface. Nevertheless, the excess of the vitamin could also alter the stoichiometry of the perovskite, affecting their own structure and photophysical properties. Consequently, 0.15-T@P1 and 0.15-T@P2 presents the optimum α-TCP concentration, see Figure 3a,b and Figure S5 (Supporting Information). For this α-TCP concentration a reduction in PLQY, after 2 months, respect the initial one of just ≈8% and 23%, respectively, see Figure 3a,b and Figure S5 (Supporting Information), while samples without α-TCP shows a 100% decrease in a short period. These results are in good agreement with the XRD patterns obtained for the PNCs in absence and presence of α-TCP for this period of time, where the stabilization of black phase in PNCs modified with the vitamin was established.

On the other hand, we analysed the mechanism of recombination dynamics of *X*-T@P1 and *X*-T@P2 in presence of α-TCP before and after 60 days under air ambient, through time-resolved PL (TRPL) measurements. We collected their corresponding average electron lifetimes, τ_{avg}.[48] observing longer $\tau_{avg,}$ when α-TCP is added, indicating that the carrier recombination is delayed, see Figure S7 and Table S2 (Supporting Information). Then, we calculated the radiative and non-radiative recombination decay rate constants, k_r and k_{nr} respectively, see Table S2 (Supporting Information). k_r is decreased by the presence of α-TCP, see Figure 3c. We propose that this behavior is caused by the filling of iodide vacancies through oxygen bonds from the vitamin. In this way, oxygen species support the passivation of non-radiative recombination trap states formed by the emergence of halide defect sites, improving the optical performance of the PNCs. At this point, it is reported that the oxygen passivation introduces new atomic orbitals, which are associated to shallow empty O 2p states near to the valence band maximum.[49–51] This can explain the delay in the carrier recombination. Interestingly, compared with an aged 0-T@P2 sample

at 0 day of the stability measurements, highest k_{nr}, the addition of the vitamin to this type of material improves its radiative channel. The latter is corroborated by obtaining a lower k_{nr} and k_{nr}/k_r ratio, see Figure 3c,d respectively, in 0.15-T@P2 at the same aging time, which is close to the lowest k_{nr} shown for 0.15-T@P1. This indicates that α-TCP decreases the density of non-radiative carrier traps through oxygen passivation. This result is in good agreement with the increase of both ($O_{total}/I+O_{total}$) and ($O_{total}/Pb+O_{total}$) ratios after α-TCP addition, estimated by XPS, confirming the compensation of halide deficiency by oxygen introduction. Accordingly, it can be concluded that the passivation of the PNCs surface by α-TCP treatment is carried out via oxygen bound, being able to fix the highly defective structure of fresh and aged PNCs, hindering the α-to-δ phase transformation, and restoring their intrinsic features.

With the aim to propose a mechanism of surface ligand passivation mediated by α-TCP, we conducted theoretical calculations through density functional theory (DFT) based on a mix of plane waves and Gaussian functions.[52] We have investigated the ability of α-TCP to passivate the $CsPbI_3$ PNCs surface, compared with conventional oleic acid, by calculating their BEs to the crystal surface in presence of a iodide vacancy. For the α-TCP molecule pictured in Figure S8a (Supporting Information), we have considered two binding situations: in the first case, the ligand is attached to a surface Pb cation by the ending oxygen atom from the phenolic ring, case I, which releases its hydrogen atom and occupies the position of a iodide vacancy; in the second case, the ligand approaches a surface Pb cation by the oxygen atom coming from the epoxy site, case II. For the oleic acid structure we consider that the oxygen atoms link to the same surface Pb cation through carboxylate anions after releasing their hydrogen atom. Additionally, for every molecule and binding situation, we have computed two systems composed of a nanocrystal (3.1 nm size) with a iodide vacancy plus ligand: in the first one the molecule is placed in the perovskite surface, see Figure S8b (Supporting Information); in the second one, the ligand is far apart from the perovskite surface, see Figure S8c (Supporting Information).

Based on the total energies of the above two systems, $E_{contact}$ and $E_{no\_contact}$, respectively, we have estimated the BEs as $E_b = E_{no\_contact} - E_{contact}$. For the oleic acid molecule, see **Figure 4**a, $E_b = 2.91$ eV. Then, α-TCP ligand in the binding case I showed an $E_b = 1.96$ eV and a covalent bond is created, see Figure 4b. However, for the α-TCP ligand in the binding case II, E_b is negative, and the passivation process is thermodynamically unfavorable, see Figure 4c. The fact that E_b from oleic acid molecule linked to PNCs surface is higher than α-TCP in case I is expected from its aliphatic nature, associated to a lesser steric hindrance on the PNCs surface compared with the vitamin. Nevertheless, the calculated BEs suggest, on one hand, that $CsPbI_3$ PNCs can be covered with both organic ligands, and on the other hand, the passivation process does not necessarily involve the exchange of oleic acid by the vitamin. This is deduced because the oleic acid is more strongly coupled to the crystal than α-TCP, and therefore, the complete ligand exchange would be thermodynamically unfavorable. Then, by calculating the corresponding chemical contribution of PNCs in absence and presence of α-TCP linked to the perovskite in case I, see Figure 4d,e respectively, we observed that the O 2p states are the new intraband gap energy levels emerged in the nanocrystals. These states are at 0.73 eV from the valence band (VB) maximum, corroborating that oxygen is introduced in halide positions.

Nuclear magnetic resonance spectroscopy (NMR) experiments were performed to corroborate the theoretical insights. The changes in the chemical environment of PNCs after the introduction of α-TCP were studied (details of the resonance assignation are addressed in supporting information). As exhibited in Figure 4f, ^{1}H NMR spectra were acquired. The molecular structures of the capping ligands involved in the passivation process are shown in Figure 4g, together with the labelling of the protons involved in the spin-spin coupling. Mainly, the peak at $\delta = 4.16$ ppm assigned to H-bonded to the O from the phenolic ring in α-TCP (1'')[53] disappears in the 0.15-T@P1 sample while keeping unchanged the characteristic ^{1}H NMR signals of OA/OLA observed in the PNCs in the absence of the vitamin.[10,54] Then, it is noted a broad signal at $\delta = 3.32$ ppm. The absence of the O-H signal indicates the deprotonation of phenolic OH from α-TCP, inducing the formation of the phenolate species. On the other hand, since other ^{1}H NMR resonances of α-TCP (mostly those related to 2'', 3'', and 4''(CH_3) 5''(CH_2)) present the same multiplicity and chemical shift values, we claim that oxygen from the epoxy ring does not mediate in the ligand passivation of PNCs, in good agreement with theoretical calculations. Therefore we can conclude that α-TCP is linked to the defective $CsPbI_3$ PNCs surface by oxygen coming from the phenolic ring, which explains the enhancement of the PL properties and stability of the nanocrystals. Concerning to epoxy ring, this is the active site to favor the reaction with acrylate monomers, which is the key factor to enhance the PL properties of 3D polymer composites, as we will describe below.

Once the ability of α-TCP to stabilize PNCs was established, it was studied the possibility of rapidly transferring the materials to solid composites with capability to be 3D printed into geometrically complex phases and thin film layers. To this end, 0.15-T@P1 nanocrystals in solution were used to prepare polymeric acrylic composites. Interestingly, the addition of α-TCP to the acrylic monomers such as butylacrylate (BA) and isobornyl acrylate (IBA) species allowed the plasticization of the final polymeric matrix,[55] as evidenced by changes in the glass transition temperature (T_g) see Figure S9 (Supporting Information). The printability of the vitamin-modified $CsPbI_3$ PNCs inks employing masked stereolithography apparatus technology has been demonstrated, generating a red-emitting $CsPbI_3$-polymer composite material with enhanced PLQY compared to the control experiments without α-TCP, see Figure S10 (Supporting Information) and **Table 1**. Consistently with the studies in solution, the presence of α-TCP increases the PLQY of PNCs embedded in the polymeric matrices from 36% (no vitamin) to 59%, see Figure S10 (Supporting Information). More interestingly is the enormous increase in stability of the α-TCP-modified composite. While the composite with PNCs without vitamin lose practically all the PLQY after 20 d of fabrication, see **Figure 5**a and Table 1, the composite with 0.15-T@P1 PNCs increases its PLQY reaching a remarkable ≈92% after 4 months, see Figure 5b and Table 1. This value is the highest one obtained for a red-emitting composite solid as far as we know.

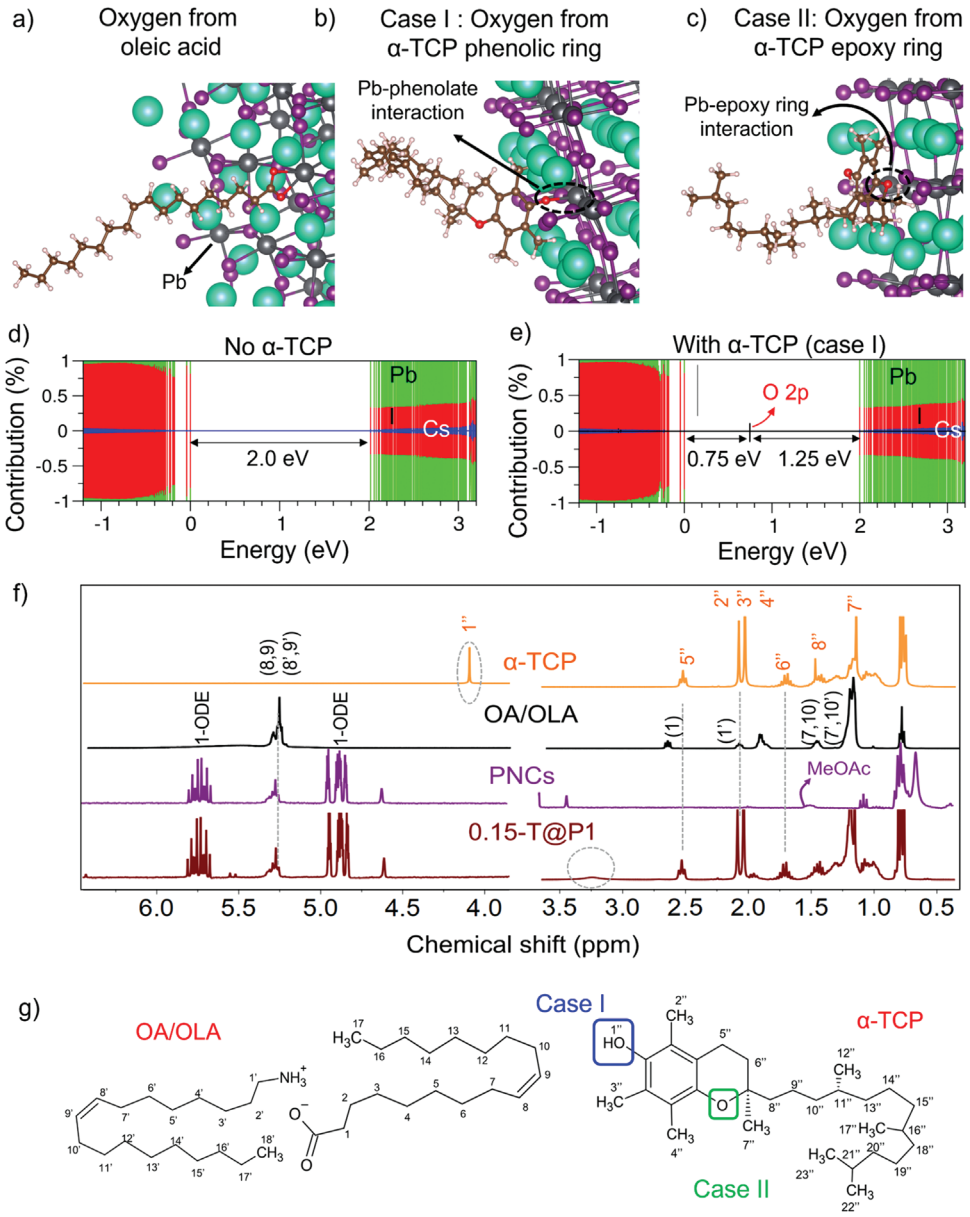

Figure 4. Representation of the organic ligands linked to PNC surface: a) oleic acid through carboxylate species, b) α-TCP molecule through oxygen from phenolic ring (binding case I), c) α-TCP molecule through oxygen from epoxy ring (binding case II). Chemical contribution from Pb (green), I (red), and Cs (blue) and oxygen (black) atomic species to the calculated molecular orbitals in PNCs showing spin-up (positive) and spin-down (negative) energy levels d) in absence and e) presence of α-TCP in binding case I. In the atomic representation a,b,c): gray, purple, and green dots refer to Pb, I, and Cs atoms, respectively. f) ^{1}H NMR spectra ($CDCl_3$, 400 MHz, 25 °C) of $CsPbI_3$ PNCs with (dark red) and without α-TCP (purple). Characteristic NMR resonances of capping ligand samples, OA/OLA mixture (black) and α-TCP (yellow), were also obtained for comparative purposes. g) Molecular structure of α-TCP and capping ligands stabilizing the PNCs.

The fabrication of a 3D acrylic composite with enhanced PLQY can be explained through DFT calculations, see Figure 5c. It is observed that filled O 2p energy states introduced by α-TCP are displaced near to the conduction band, while empty O 2p energy levels emerge, both in presence of acrylate species. Theoretically, the epoxy group of α-TCP can react with electron-rich species, e.g., negative formal charged oxygen from acrylate species, under soft synthetic conditions (30–60 °C, 20–90 min). Electron-rich species act as a nucleophile, promoting an attack over the electrophile sp^3 carbon contained into the ring.[56] The product of the ring cleavage is the formation of an alcoholate species. This hypothesis should explain the increase of energy in the filled O 2p energy states, associated to the destabilization of α-TCP structure by opening ring reaction or a strong interaction with the acrylate. Interestingly, the formation of alcoholate species shows a high affinity to surface Cs^+ from PNCs, (seen in computational calculations) transferring electrons to this metal. This suggests that O 2p orbitals are depopulated by electrons, generating empty energy levels. In this context, more electrons coming from the

Table 1. Comparison PL parameters over time for 0-T@P1 and 0.15-T@P1 acrylic composites in the absence and presence of α-TCP. PLQY values were obtained in 0–1 range.

Samples	Quantum Yield	PL peak [nm]
0-T@P1		
1 day	0.36	684.4
20 days	0.03	676.2
0.15-T@P1		
1 day	0.59	687.7
120 days	0.92	695.5

Cs-O interaction can be accumulated into PNCs, facilitating the electron transition to empty energy levels at lower energy. This could explain the nearly double value of PLQY of the 3DP solid containing α-TCP compared to the composite without α-TCP.

To strengthen the conception about the epoxy ring cleavage hypothesis, ^{1}H-NMR spectra for PNCs combined with both BA, IBA, see Figure S11a,b (Supporting Information) respectively, and the mixture of these acrylic monomers were also acquired, See Figure 5d (resonance assignation is shown in supporting information). Considering that PNCs are embedded into an acrylate matrix, it is expected to evidence the characteristic NMR signals of each monomer, mainly those from protons bonded to C=C, and multiplets coming from protons in butyl and isobornyl substituents in BA and IBA,[57] respectively. Nevertheless, changes in main signals coming from α-TCP were also observed. Singlets corresponding to methyl components bonded to the phenolic ring (3'',4'') (δ = 2.11 ppm) become a doublet, with a upfield shift to δ = 2.05 and 2.03 ppm, respectively. This fact indicates that the chemical environment of both the substituents has been modified, coupling of two kinds of protons. Then, the triplet from CH_2 in position 5'' also move upfield from δ = 2.60 to 2.53 ppm. In this context, the results suggest that the epoxy ring can be opened under the conditions assayed by effect of BA and IBA.

Then, by studying the monomer mixture without and with α-TCP, see Figure 5d, the signals referred as CH_3 doublet (3'',4'') and triplet from CH_2 (5') are also detailed in the corresponding NMR features. This fact allows to infer that the epoxy ring cleavage is conducted under the co-existence of both acrylate species. Interestingly, the multiplicity of some of the signals coming from CH_3 (3'',4'') changes in presence of the PNCs see BA/IBA-0.15-T@P1 in Figure 5d. This is a strong indication that the chemical environment of the α-TCP is widely altered by the influence of the PNCs, which could be ascribed to the interaction between the nanocrystal surface, the metal cations

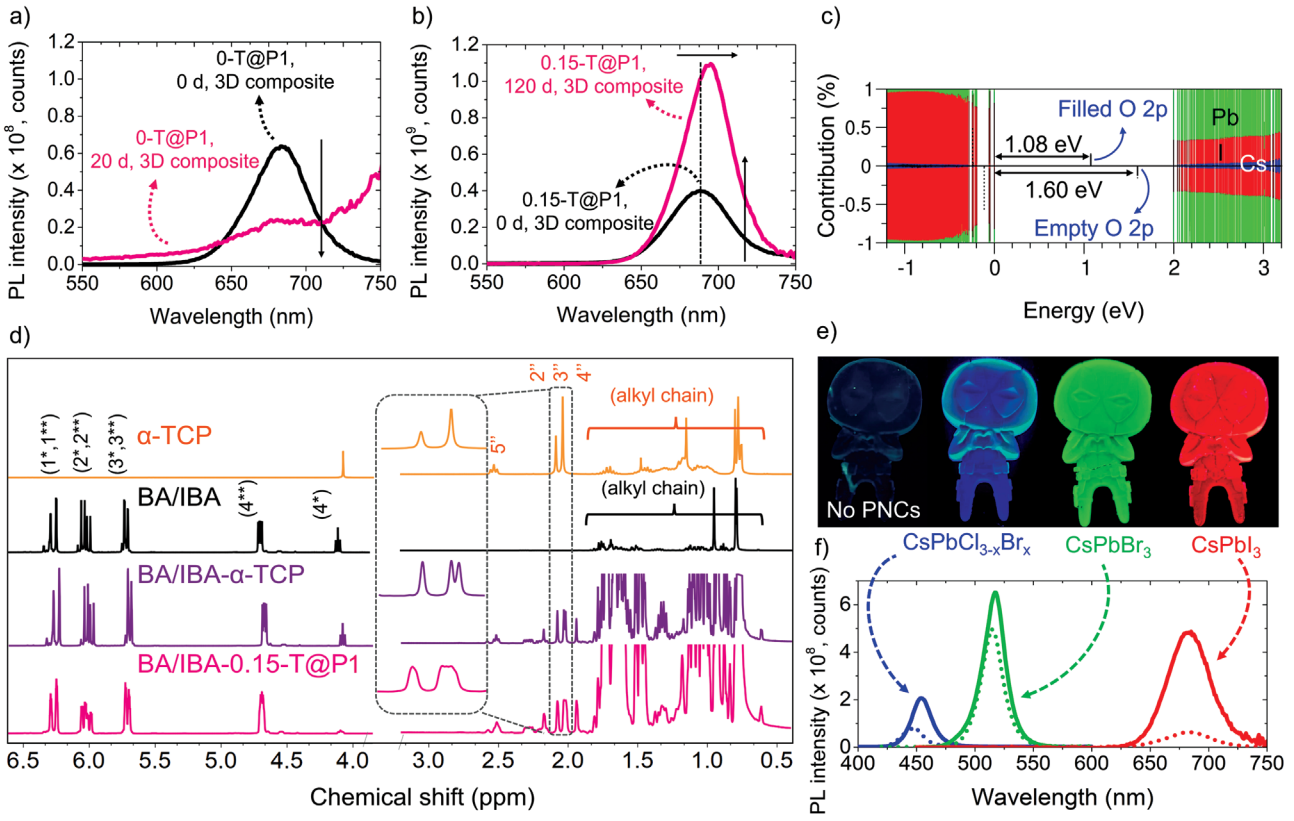

Figure 5. PL features of a) as-prepared 0-T@P1 and b) 0.15-T@P1 3D acrylic composites by exposed to the ambient air at different times: day 0 (black line), 20 and 120 d for the composites in absence and presence of α-TCP, respectively (magenta line). c) Chemical contribution from Pb (green), I (red), and Cs (blue) and oxygen (black) atomic species to the calculated molecular orbitals in in a 0.15-T@P1-acrylate composite, showing spin-up (positive) and spin-down (negative) energy levels. d) ^{1}H NMR spectra (CDCl3, 400 MHz, 25 °C) of α-TCP (yellow) BA/IBA (black), BA/IBA-α-TCP (purple) and BA/IBA-0.15-T@P1 (pink) systems. g) Photograph of as-prepared α-TCP@$CsPbX_3$ PNCs-acrylic 3D composite by varying the halide composition under UV light. f) PL spectra of the luminescent composites in absence (short dot) and presence (solid line) of α-TCP.

or the iodide species, and both monomers, being these specific to the experimental conditions employed. Indeed, a systematic ^{1}H NMR study with different proportions between the IBA monomer and α-TCP reinforced the hypothesis of α-TCP structural modification in presence of acrylates, see Figure S12 (Supporting Information). Additional NMR analysis (^{13}C, HSQC and HMBC) can be found in the supporting information, see Figures S13–S15 (Supporting Information). It is suggested that PNCs serve as a catalyst to induce the reaction between BA, IBA, and α-TCP, which does not occur when the photomaterial is separately combined with BA or IBA. These facts point to a three-side synergistic effect between PNCs, α-TCP and BA or IBA able to boost PLQY and long-term stability of PNCs/polymer composites.

Ultimately, the PL wavelength of luminescent 3D composites can be modulated throughout the visible spectra as a function of the halide nature into the $CsPbX_3$ PNCs (X = Cl, Br, I, and halide combinations). Following the route to obtain red-emitting α-TCP@$CsPbI_3$ PNCs, we have prepared α-TCP@$CsPbCl_{3-x}Br_x$ (nominal Cl:Br molar ratio = 1:1) and α-TCP@$CsPbBr_3$ PNCs, observing the typical blue and green emission in the 3D printed acrylic composite materials, see Figure 5e, with a higher PL intensity compared with those in absence of α-TCP, see Figure 5f. This behavior was accompanied with a redshift in the PL peak position. Considering that ionic radius of halides increases as follows: $Cl^- < Br^- < I^-$, we suggest that the incorporation of oxygen from α-TCP can enlarge the perovskite lattice with smaller halide, causing the change in the PL feature. Accordingly, we deduce that the passivation effect provided by α-TCP is useful to prepare PNCs inks with a wide halide composition, providing multicolour 3D polymeric solids. At this stage, it can be concluded that α-TCP offers the preparation of high stable and compatible to $CsPbX_3$ PNCs solutions for fabricating 3D printing polymeric materials with good mechanical and photophysical properties, see Figure 5e, opening the door to alternatives for obtaining diverse active layer for robust optoelectronics.

3. Conclusion

A natural and non-toxic active agent, based on tocopherol, has been employed in post-synthetic treatments of PNCs to improve their photophysical properties for the first time. The addition of vitamin increases photoluminescent emission of blue, green and red emitting PNCs. Among them, the red emitting $CsPbI_3$ are the ones with more demanding requirements in terms of stability due to the poor black perovskite phase stability. The properties of α-TCP have been demonstrated on as-prepared and on aged perovskites, effectively restoring the reduced photophysical properties due to the formation of surface defects. We elucidated that α-TCP promotes an efficient surface passivation of defective $CsPbI_3$ PNCs, filling iodide vacancies through oxygen incorporation coming from phenolic ring composing the vitamin structure. Accordingly, non-radiative electron traps are suppressed, facilitating the radiative channel for carrier relaxation. This fact allows to achieve a PLQY up to 100% in the PNCs, keeping stable the black phase for 2 months under ambient air. Based on these characteristics, we were able to prepare inks with α-TCP-PNCs and acrylate-based monomers for the efficient 3D printing of polymer-PNC photoluminescent composites. Photoluminescent 3D printed composites achieved a 92% PLQY after 4 months, to the best of our knowledge, the highest value obtained for a PNC red-emissive composite until now. A potential reaction between α-TCP and acrylate monomers during the composite fabrication promotes electron transfer from the oxygenated species to the PNCs. This fact generates empty O 2p states near to the conduction band, and the accumulation of more electrons into the semiconductor. At this point, electron transitions can be facilitated at lower energy, favoring the radiative carrier recombination dynamics, reason to unlock the enhanced PL features of the acrylate composite. This approach has been extrapolated to other PNCs by varying the halide composition, reaching the fabrication of multicolor polymeric composites. According to the above results, we provide an attractive strategy to facilitate the manufacture of highly photoluminescent devices through 3D printing, with diverse and more complex geometries, and the preparation of stable and compatible PNCs inks with improved PL properties for inkjet printing applications.

Supporting Information

Supporting Information is available from the Wiley Online Library or from the author.

Acknowledgements

This work was supported by European Research Council (ERC) via Consolidator Grant (724424–No-LIMIT), Spanish Ministry of Science and Innovation under projects STABLE (PID2019-107314RB-I00) and NIRVANA (PID2020-119628RB-C33), Generalitat Valenciana via Prometeo Grant Q-Solutions (CIPROM/2021/078) and CIDEGENT (2018/036); and the Agencia Valenciana de Innovación (AVI) (INNCON/2021/13, INNVA/2022/9). M.Z. thanks Marie Skłodowska-Curie Individual Fellowships (GA no. 101026335) for funding. The authors also thank to Ministry of Education, Youth and Sports of the Czech Republic for the financial support of XPS measurements using CEMNAT infrastructure (project LM 2018103). The authors are very grateful to the "Serveis Centrals d'Instrumentació Científica (SCIC)" of the Universitat Jaume I.

Author Contributions

I.R. and A.F.G.-R. contributed equally to this work. I.M.-S. and V.S. conceived the project. I.R and A.F.G.-R. designed the experiments. A.F.G.-R. and A.V.-A. synthesized PNCs and performed the corresponding morphological, structural, and optical properties. I.R. formulated, prepared and chracterised the composite structures. I.R. and J.S. fabricated the PNCs-composites. I.R. conducted the photophysical characterization of the PNCs-composites. C.E.-A. performed the theoretical calculations. J.R.-P. contributed to the XPS measurements and analysis. I.R and M.Z. conducted the NMR analysis. I.R and A.F.G.-R. coordinated the experimental work. I.M.-S. and V.S. coordinated the whole project. A.F.G.-R., I.R., I.M.-S., and V.S. wrote the manuscript. All the authors contributed to the discussions.

Conflict of Interest

The authors declare no conflict of interest.

Data Availability Statement

The data that support the findings of this study are available from the corresponding author upon reasonable request.

Keywords

3D printing, additive manufacturing, halide perovskites, nanocrystals, polymer, stability

Received: September 16, 2022
Revised: October 28, 2022
Published online:

[1] L. Protesescu, S. Yakunin, M. I. Bodnarchuk, F. Krieg, R. Caputo, C. H. Hendon, R. X. Yang, A. Walsh, M. V. Kovalenko, *Nano Lett.* **2015**, *15*, 3692.
[2] L. C. Schmidt, A. Pertegás, S. González-Carrero, O. Malinkiewicz, S. Agouram, G. Mínguez Espallargas, H. J. Bolink, R. E. Galian, J. Pérez-Prieto, *J. Am. Chem. Soc.* **2014**, *136*, 850.
[3] A. Dey, J. Ye, A. De, E. Debroye, S. K. Ha, E. Bladt, A. S. Kshirsagar, Z. Wang, J. Yin, Y. Wang, L. N. Quan, F. Yan, M. Gao, X. Li, J. Shamsi, T. Debnath, M. Cao, M. A. Scheel, S. Kumar, J. A. Steele, M. Gerhard, L. Chouhan, K. Xu, X.-g. Wu, Y. Li, Y. Zhang, A. Dutta, C. Han, I. Vincon, A. L. Rogach, et al., *ACS Nano* **2021**, *15*, 10775.
[4] A. F. Gualdrón-Reyes, D. F. Macias-Pinilla, S. Masi, C. Echeverría-Arrondo, S. Agouram, V. Muñoz-Sanjosé, J. Rodríguez-Pereira, J. M. Macak, I. Mora-Seró, *J. Mater. Chem. C* **2021**, *9*, 1555.
[5] F. Liu, Y. Zhang, C. Ding, S. Kobayashi, T. Izuishi, N. Nakazawa, T. Toyoda, T. Ohta, S. Hayase, T. Minemoto, K. Yoshino, S. Dai, Q. Shen, *ACS Nano* **2017**, *11*, 10373.
[6] A. F. Gualdrón-Reyes, S. Masi, I. Mora-Seró, *Trends Chem.* **2021**, *3*, 499.
[7] X. Du, G. Wu, J. Cheng, H. Dang, K. Ma, Y.-W. Zhang, P.-F. Tan, S. Chen, *RSC Adv.* **2017**, *7*, 10391.
[8] L. Protesescu, S. Yakunin, S. Kumar, J. Bär, F. Bertolotti, N. Masciocchi, A. Guagliardi, M. Grotevent, I. Shorubalko, M. I. Bodnarchuk, C.-J. Shih, M. V. Kovalenko, *ACS Nano* **2017**, *11*, 3119.
[9] M. I. Bodnarchuk, S. C. Boehme, S. ten Brinck, C. Bernasconi, Y. Shynkarenko, F. Krieg, R. Widmer, B. Aeschlimann, D. Günther, M. V. Kovalenko, I. Infante, *ACS Energy Lett.* **2018**, *4*, 63.
[10] E. Hassanabadi, M. Latifi, A. F. Gualdrón-Reyes, S. Masi, S. Y. joon, M. Poyatos, B. Julián-López, I. M. Seró, *Nanoscale* **2020**, *12*, 14194.
[11] A. Swarnkar, A. R. Marshall, E. M. Sanehira, B. D. Chernomordik, D. T. Moore, J. A. Christians, T. Chakrabarti, J. M. Luther, *Science* **2016**, *354*, 92.
[12] S. Masi, A. F. Gualdrón-Reyes, I. Mora-Seró, *ACS Energy Lett.* **2020**, *5*, 1974.
[13] A. Dutta, S. K. Dutta, S. Das Adhikari, N. Pradhan, *ACS Energy Lett.* **2018**, *3*, 329.
[14] S. Ma, S. H. Kim, B. Jeong, H.-C. Kwon, S.-C. Yun, G. Jang, H. Yang, C. Park, D. Lee, J. Moon, *Small* **2019**, *15*, 1900219.
[15] Z. Li, M. Yang, J.-S. Park, S.-H. Wei, J. J. Berry, K. Zhu, *Chem. Mater.* **2016**, *28*, 284.
[16] W. Shockley, H. J. Queisser, *J. Appl. Phys.* **1961**, *32*, 510.
[17] M. Albaladejo-Siguan, E. C. Baird, D. Becker-Koch, Y. Li, A. L. Rogach, Y. Vaynzof, *Adv. Energy Mater.* **2021**, *11*, 2003457.
[18] R. Han, Q. Zhao, J. Su, X. Zhou, X. Ye, X. Liang, J. Li, H. Cai, J. Ni, J. Zhang, *J. Phys. Chem. C* **2021**, *125*, 8469.
[19] E. M. Sanehira, A. R. Marshall, J. A. Christians, S. P. Harvey, P. N. Ciesielski, L. M. Wheeler, P. Schulz, L. Y. Lin, M. C. Beard, J. M. Luther, *Sci. Adv.* **2017**, *3*, eaao4204.
[20] Y. Zhang, T. D. Siegler, C. J. Thomas, M. K. Abney, T. Shah, A. De Gorostiza, R. M. Greene, B. A. Korgel, *Chem. Mater.* **2020**, *32*, 5410.
[21] S. Seth, T. Ahmed, A. De, A. Samanta, *ACS Energy Lett.* **2019**, *4*, 1610.
[22] S. Masi, A. F. Gualdrón-Reyes, I. Mora-Seró, *ACS Energy Lett.* **2020**, *5*, 1974.
[23] P. K. Nayak, M. Sendner, B. Wenger, Z. Wang, K. Sharma, A. J. Ramadan, R. Lovrinčić, A. Pucci, P. K. Madhu, H. J. Snaith, *J. Am. Chem. Soc.* **2018**, *140*, 574.
[24] K. A. Huynh, S.-R. Bae, T. V. Nguyen, H. H. Do, D. Y. Heo, J. Park, T.-W. Lee, Q. V. Le, S. H. Ahn, S. Y. Kim, *ACS Photonics* **2021**, *8*, 1979.
[25] H. Wang, N. Sui, X. Bai, Y. Zhang, Q. Rice, F. J. Seo, Q. Zhang, V. L. Colvin, W. W. Yu, *J. Phys. Chem. Lett.* **2018**, *9*, 4166.
[26] T. D. Ngo, A. Kashani, G. Imbalzano, K. T. Q. Nguyen, D. Hui, *Composites, Part B* **2018**, *143*, 172.
[27] A. Ambrosi, M. Pumera, *Chem. Soc. Rev.* **2016**, *45*, 2740.
[28] D. J. Wales, Q. Cao, K. Kastner, E. Karjalainen, G. N. Newton, V. Sans, *Adv. Mater.* **2018**, *30*, 1800159.
[29] M. Gastaldi, I. Roppolo, A. Chiappone, C. Garino, A. Fin, M. Manachino, P. Sirianni, G. Viscardi, L. Scaltrito, M. Zanetti, S. Bordiga, C. Barolo, *Addit. Manuf.* **2022**, *49*, 102504.
[30] D. J. Wales, Q. Cao, K. Kastner, E. Karjalainen, G. N. Newton, V. Sans, *Adv. Mater.* **2018**, *30*, 1800159.
[31] S. Y. Lee, G. Lee, D. Y. Kim, S. H. Jang, I. Choi, J. Park, H.-K. Park, J. W. Jung, K. H. Cho, J. Choi, *APL Photonics* **2021**, *6*, 056104.
[32] J. Ahn, S. Jeon, H. K. Woo, J. Bang, Y. M. Lee, S. J. Neuhaus, W. S. Lee, T. Park, S. Y. Lee, B. K. Jung, H. Joh, M. Seong, J.-h. Choi, H. G. Yoon, C. R. Kagan, S. J. Oh, *ACS Nano* **2021**, *15*, 15667.
[33] F. Cheng, X. Jing, R. Chen, J. Cao, J. Yan, Y. Wu, X. Huang, B. Wu, N. Zheng, *Inorg. Chem. Front.* **2019**, *6*, 2458.
[34] J.-W. Lee, Z. Dai, C. Lee, H. M. Lee, T.-H. Han, N. De Marco, O. Lin, C. S. Choi, B. Dunn, J. Koh, D. Di Carlo, J. H. Ko, H. D. Maynard, Y. Yang, *J. Am. Chem. Soc.* **2018**, *140*, 6317.
[35] A. Kamal-Eldin, L.-Å. Appelqvist, *Lipids* **1996**, *31*, 671.
[36] Q. Zhang, H. Nan, Y. Zhou, Y. Gu, M. Tai, Y. Wei, F. Hao, J. Li, D. Oron, H. Lin, *J. Mater. Chem. C* **2019**, *7*, 6795.
[37] J. Satta, C. Melis, C. M. Carbonaro, A. Pinna, M. Salado, D. Salazar, P. C. Ricci, *J. Materiomics* **2021**, *7*, 127.
[38] J.-K. Sun, S. Huang, X.-Z. Liu, Q. Xu, Q.-H. Zhang, W.-J. Jiang, D.-J. Xue, J.-C. Xu, J.-Y. Ma, J. Ding, Q.-Q. Ge, L. Gu, X.-H. Fang, H.-Z. Zhong, J.-S. Hu, L.-J. Wan, *J. Am. Chem. Soc.* **2018**, *140*, 11705.
[39] X. Zheng, Y. Hou, H.-T. Sun, O. F. Mohammed, E. H. Sargent, O. M. Bakr, *J. Phys. Chem. Lett.* **2019**, *10*, 2629.
[40] C. Zhang, Q. Wan, L. K. Ono, Y. Liu, W. Zheng, Q. Zhang, M. Liu, L. Kong, L. Li, Y. Qi, *ACS Energy Lett.* **2021**, *6*, 3545.
[41] Q. Zhao, A. Hazarika, L. T. Schelhas, J. Liu, E. A. Gaulding, G. Li, M. Zhang, M. F. Toney, P. C. Sercel, J. M. Luther, *ACS Energy Lett.* **2019**, *5*, 238.
[42] A. F. Gualdrón-Reyes, J. Rodríguez-Pereira, E. Amado-González, J. Rueda-P, R. Ospina, S. Masi, S. J. Yoon, J. Tirado, F. Jaramillo, S. Agouram, V. Muñoz-Sanjosé, S. Giménez, I. Mora-Seró, *ACS Appl. Mater. Interfaces* **2020**, *12*, 914.
[43] C. Lee, Y. Shin, A. Villanueva-Antoli, S. Das Adhikari, J. Rodríguez-Pereira, J. M. Macak, C. Mesa, S. J. Yoon, A. F. Gualdrón-Reyes, I. M. Seró, *Chem. Mater.* **2021**, *33*, 8745.
[44] A. Swarnkar, A. R. Marshall, E. M. Sanehira, B. D. Chernomordik, D. T. Moore, J. A. Christians, T. Chakrabarti, J. M. Luther, *Science* **2016**, *354*, 92.
[45] Y. Shynkarenko, M. I. Bodnarchuk, C. Bernasconi, Y. Berezovska, V. Verteletskyi, S. T. Ochsenbein, M. V. Kovalenko, *ACS Energy Lett.* **2019**, *4*, 2703.

[46] J. Pan, Y. Shang, J. Yin, M. De Bastiani, W. Peng, I. Dursun, L. Sinatra, A. M. El-Zohry, M. N. Hedhili, A.-H. Emwas, O. F. Mohammed, Z. Ning, O. M. Bakr, *J. Am. Chem. Soc.* **2017**, *140*, 562.
[47] F. Krieg, S. T. Ochsenbein, S. Yakunin, S. ten Brinck, P. Aellen, A. Süess, B. Clerc, D. Guggisberg, O. Nazarenko, Y. Shynkarenko, S. Kumar, C.-J. Shih, I. Infante, M. V. Kovalenko, *ACS Energy Lett.* **2018**, *3*, 641.
[48] J.-S. Yao, J. Ge, K.-H. Wang, G. Zhang, B.-S. Zhu, C. Chen, Q. Zhang, Y. Luo, S.-H. Yu, H.-B. Yao, *J. Am. Chem. Soc.* **2019**, *141*, 2069.
[49] S.-C. Liu, Z. Li, Y. Yang, X. Wang, Y.-X. Chen, D.-J. Xue, J.-S. Hu, *J. Am. Chem. Soc.* **2019**, *141*, 18075.
[50] R. Brenes, C. Eames, V. Bulović, M. S. Islam, S. D. Stranks, *Adv. Mater.* **2018**, *30*, 1706208.
[51] W. Fan, Y. Shi, T. Shi, S. Chu, W. Chen, K. O. Ighodalo, J. Zhao, X. Li, Z. Xiao, *ACS Energy Lett.* **2019**, *4*, 2052.
[52] J. P. Perdew, K. Burke, M. Ernzerhof, *Phys. Rev. Lett.* **1996**, *77*, 3865.
[53] ChemicalBook, https://www.chemicalbook.com/SpectrumEN_10191-41-0_1HNMR.htm (accessed: November 2021).
[54] R. Grisorio, M. E. Di Clemente, E. Fanizza, I. Allegretta, D. Altamura, M. Striccoli, R. Terzano, C. Giannini, M. Irimia-Vladu, G. P. Suranna, *Nanoscale* **2019**, *11*, 986.
[55] K. Matyjaszewski, J. Xia, *Chem. Rev.* **2001**, *101*, 2921.
[56] A. V. Reis, A. R. Fajardo, I. T. A. Schuquel, M. R. Guilherme, G. J. Vidotti, A. F. Rubira, E. C. Muniz, *J. Org. Chem.* **2009**, *74*, 3750.
[57] SDBS, https://sdbs.db.aist.go.jp/sdbs/cgi-bin/direct_frame_top.cgi (accessed: November 2021).